Transport Rectification in Nanopores with Outer Membranes Modified with Surface Charges and Polyelectrolytes

Mario Tagliazucchi,[†] Yitzhak Rabin,[‡] and Igal Szleifer[†,*]

[†]Department of Biomedical Engineering, Department of Chemistry and Chemistry of Life Processes Institute, Northwestern University, Evanston, Illinois 60208, United States and [‡]Department of Physics and Institute for Nanotechnology and Advanced Materials, Bar-Ilan University, Ramat-Gan 52900, Israel

ABSTRACT This work reports a comprehensive theoretical study of the transport-rectification properties of cylindrical nanopores with neutral inner walls and chemically modified outer membrane. The chemical species on the two outer sides of the membrane have charges of opposite sign and can be either surface-confined species (*i.e.*, surface charges) or polyelectrolyte brushes. The advantage of this design over other types of rectifying nanopores is that it requires controlling the composition of the outer walls of the pore (which are easy to access) rather than the inner walls, thus simplifying the fabrication process. Ion-current rectification in nanopores with charged outer walls is ascribed to applied-potential-induced changes in the ionic concentration within the pore. The rectification efficiency is studied as a function of pore length, radius, surface charge and bulk electrolyte concentration. An analytical model is derived for the case of surface-confined charges that predicts the current–potential curves in very good agreement with the numerical calculations. Neutral nanopores with polyelectrolyte-modified outer walls have two distinct advantages compared to surface-charged systems: (i) they exhibit higher rectification factors due to the large charge density immobilized by the polyelectrolyte brushes, and (ii) the applied potential deforms the polyelectrolyte chains toward the oppositely charged electrode. This deformation brings the polyelectrolyte brushes into the pore in the low conductivity state and expels them from the pore in the high conductivity regime. Calculations of the potentials of mean-force suggest that the applied-field-induced conformational changes can be used to control the translocation of cargoes larger than ions, such as proteins and nanoparticles.

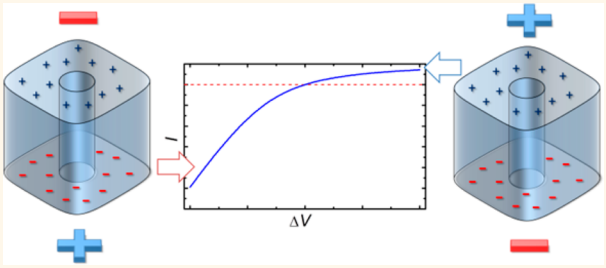

KEYWORDS: nanochannel · nanofluidics · diode · concentration polarization · electrostatics · nonequilibrium

Future nanofluidic devices will be assemblies of nanopores and nanochannels integrated into logical networks, in analogy to current electronic circuits. Nanofluidic components equivalent to electronic diodes[1,2] and transistors[2−4] have already been fabricated. Transport-rectifying nanopores and nanochannels, the nanofluidic equivalents to electronic diodes, find applications in sensing,[5−10] nanofluidic circuits,[11,12] energy conversion[11,13−15] and nanoelectrochemistry.[1,16,17] Ionic rectification requires breaking the symmetry of the system;[1,18] the asymmetry can be geometrical (*e.g.*, conical nanopores/channels[5−7,10,12,19−24]), from differences in the compositions of the reservoirs[24,25] or be originated in an asymmetrical charge distribution in an otherwise symmetrical system, *e.g.*, a cylindrical nanopore with inner walls that are charged positively in one half of the pore and negatively in the other half.[2,4,15,26−31] Daiguji *et al.*[4] and Vlassiouk *et al.*[31] have analyzed systematically the latter case, known as the bipolar diode, and they showed that this design has excellent rectification properties. However, experimental implementation of the bipolar diode requires fine control over the charge density distribution of the inner walls, which can be a very challenging task for current nanofabrication techniques. One can imagine an alternative design, where the inner walls of the nanopore are electrically neutral but the outer walls have been chemically modified to introduce charges of opposite sign on each side of the membrane, either in the form of surface charges (surface-charged outer walls, Figure 1A) or end-grafted polyelectrolytes (polyelectrolyte-modified outer walls, Figure 1B). These designs are attractive because the surfaces of the membrane can be modified before drilling or etching the pore.

* Address correspondence to igalsz@northwestern.edu.

Received for review July 17, 2013 and accepted September 18, 2013.

Published online September 18, 2013
10.1021/nn403686s

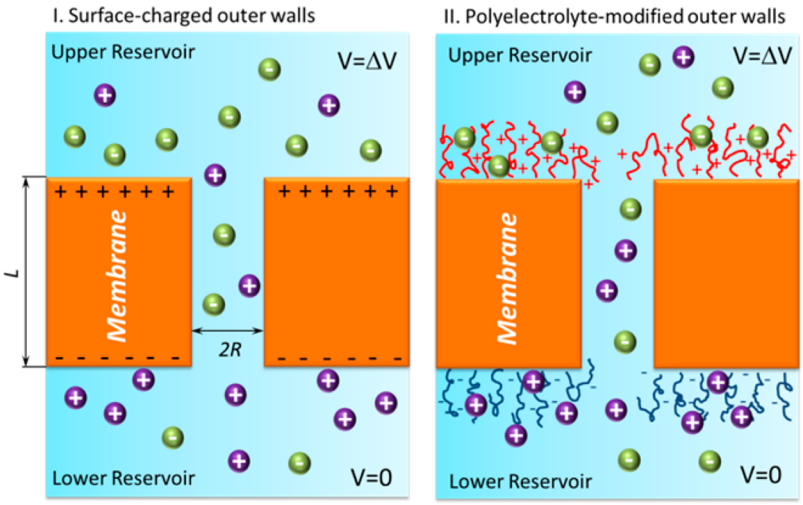

Figure 1. The system under study is a cylindrical pore of length *L* and radius *R* drilled in a membrane. The inner walls of the pore are neutral and the outer walls have charges of opposite sign but equal surface density. These charges are either due to a surface charge density (surface-charged outer walls, left) or end-grafted polyelectrolyte brushes (polyelectrolyte-modified outer walls, right). The pore connects two infinite reservoirs containing a c^{bulk} concentration of monovalent cations (C) and anions (A), as well as solvent molecules (water). The charge density in the surface-charged outer wall system is σ_q. The polyelectrolytes in the polyelectrolyte-modified system are grafted with a surface density σ_{pol} and bear *N* segments per chain; each segment has a charge *f* (*f* = ±1/3 |*e*| in all calculations in this work). Applying a potential difference ΔV between reversible electrodes located in the bulk solutions of the reservoirs gives rise to an ionic current of intensity *I* (we adopt the convention $V \equiv 0$ for the lower reservoir).

The current-rectification properties of these appealing systems remain mainly unexplored as neutral nanopores with charged outer walls have been explored only very briefly in the literature[31] and nanopores with polyelectrolyte-modified outer walls have not been addressed at all.

This work is a comprehensive study of the current response and molecular organization of rectifying nanopores with chemically modified outer walls. We model these systems using a steady-state molecular theory developed in our previous publication.[32] Our theory explicitly accounts for the coupling between nonequilibrium ion fluxes, polyelectrolyte conformations, electrostatic and nonelectrostatic interactions and the volume, charge, size and charge distribution of all molecular species in the system. In previous work, we have shown that the theory predicts the pH-dependent conductance of polyelectrolyte-modified long nanochannels in very good agreement with experimental observations.[33] We apply here the theory to study nanopores with outer walls modified by surface charges and polyelectrolyte brushes and show that current rectification arises from the changes in ionic concentration within the pore due to the applied potential. We also introduce a simple analytical model, for the case of surface-confined charges, which describes the current–potential curves in excellent agreement with the numerical predictions of the theory and, therefore, can be used as a designing tool for experiments. Our results reveal two unique properties of nanopores with polyelectrolyte-modified outer walls: (i) these pores show rectification ratios much larger than those exhibited by the surface-charged case because polyelectrolyte chains immobilize a very high charge density and their flexibility allows them to explore the interior of the pore and (ii) the applied potential drives the polyelectrolytes into the pore in the low-current state and out of the pore in the high current-state. On the basis of these potential-induced conformational changes, we propose that nanopores with polyelectrolyte-modified outer walls can behave as electromechanical gates.

One of the main findings of the present work is that high current rectification factors are observed even when the dimensions of the pore exceed the length scale of the electrostatic interactions (the Debye length). In other words, the presence of charged outer walls does not affect the electrostatic environment within the pore in equilibrium; however, under an applied potential (*i.e.*, non-equilibrium conditions), the charges on the outer walls dictate the internal molecular organization of the pore. This result demonstrates the need to develop new intuition for nonequilibrium systems, as many of the concepts derived for equilibrium conditions are no longer applicable.

RESULTS AND DISCUSSIONS

Current Rectification in Neutral Nanopores with Charged Outer Surfaces Is Caused by Potential-Induced Changes in the Salt Concentration within the Pore. Figure 2 shows a current–potential curve for a nanopore with neutral inner walls and surface-charged outer walls (system shown in Figure 1I), calculated with the molecular theory. The dimensions of the pore (L = 20 nm, R = 7.5 nm) are consistent with the dimensions of solid-state nanopores drilled in ultrathin Si_3N_4 membranes[34,35]

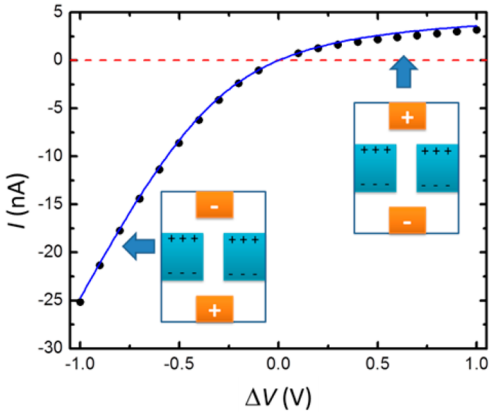

Figure 2. Current−potential plot for a pore with surface-charged outer walls (symbols, numerical solution of the nonequilibrium molecular theory; solid blue line, analytical model). The figure shows the polarity of the membrane charges and potential biases applied to the electrodes in the reservoirs for the '*on*' state ($\Delta V < 0$) and the '*off*' state ($\Delta V > 0$). Calculation parameters: $L = 20$ nm, $R = 7.5$ nm, $\sigma_q = 0.5\ |e|\cdot nm^{-2}$, $c^{bulk} = 0.1$ M.

(the effect of pore dimensions is discussed below). The density of charges on the outer walls ($\sigma_q = 0.5\ |e|\cdot nm^{-2}$) is within the range observed for thiol self-assembled monolayers[36] and metal oxide surfaces.[29] Figure 2 shows that the current is larger for $\Delta V < 0$ (the *on* state, where the positively charged outer wall faces the negatively biased electrode) than for $\Delta V > 0$ (the *off* state, where the positively charged outer wall faces the positively biased electrode). The efficiency of the rectification is quantified by the current rectification factor, $\alpha(|\Delta V|) = -I(-\Delta V)/I(\Delta V)$ (a nonrectifying, ohmic system has $\alpha \equiv 1$). For the curve in Figure 2, $\alpha(|\Delta V| = 0.5\ V)$ is 4.0.

Current rectification in a neutral nanopore with charged outer walls is a consequence of the changes in the concentration of salt ions within the nanochannel due to the applied potential. Potential-induced reorganization of salt ions occurs in other nanopore and nanochannel systems exhibiting nonohmic behaviors, including rectifying nanopores.[2,4,31,32,37,38] Figure 3A shows color maps for the concentration of anions and cations in a plane perpendicular to the membrane for different applied potentials: $\Delta V = 0$ V (equilibrium), 0.5 V, and −0.5 V. In equilibrium, the influence of the charges on the outer walls is limited to the thickness of the electrical double layer, which is of the order of the Debye length (~1 nm for the 0.1 M electrolyte used in the calculations of Figures 2 and 3). Therefore, the salt concentration inside the nanopore for $\Delta V = 0$ V is equal to the bulk salt concentration (0.1 M). The concentration of ions within the pore for $\Delta V = 0.5$ V (*off* state) is lower than the bulk concentration, while that for $\Delta V = -0.5$ V (*on* state) is larger than the bulk concentration. Current rectification is explained by the fact that the electrical resistance of the pore decreases as its internal salt concentration increases; therefore, the currents for negative applied

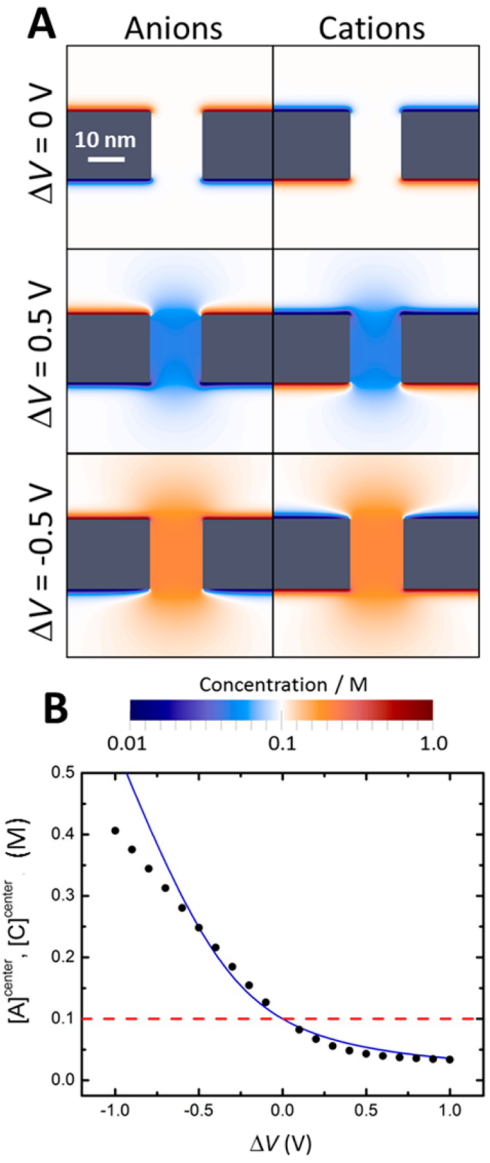

Figure 3. (A) Color maps of anion and cation concentrations along a plane containing the pore axis for different applied biases. (B) Concentration of anions and cations in the center of the pore ($r = 0$, $z = L/2$) as a function of the applied potential (the concentration of anions and cations is the same); symbols and the solid blue line show the prediction of the nonequilibrium molecular theory and the analytical model, eq 2, respectively. The dashed red line shows the bulk salt concentration, $c^{bulk} = 0.1$ M. Same calculation parameters as in Figure 2.

potentials (concentration enhancement) are larger than those for positive applied potentials (concentration depletion). Note that Figure 3A shows that the concentrations of anions and cations within the pore remain always equal to each other, which is expected from the symmetry of the system and the fact that separating electrical charges results in a very large associated energetic penalty. Observe also that the spatial region where the salt concentration changes spans the interior of the pore and the hemispherical region at both entrances but not the reservoirs. In Figure 3B, we plot

the concentration in the center of the pore as a function of the applied potential. This figure shows that the potential-induced concentration changes can be very large: the salt concentration inside the pore decreases by a factor of approximately 3 when applying a potential of +1 V and increases a factor of 4 when applying a bias of −1 V.

The changes in the salt concentration with applied potential observed in Figure 3 can be rationalized by considering the interaction of the ions flowing through the system with the charges on the outer walls. In the *on* state, the cations flow from the lower reservoir (which has negatively charged outer walls) into the pore and then into the upper reservoir (which has positively charged outer walls). The high concentration of charge carriers (cations) near the negatively charged membrane in the lower reservoir causes the electrical resistance of the 'entrance' reservoir (the lower reservoir) to be smaller than that of the 'exit' reservoir (the upper reservoir). Therefore, the migration flux of cations (*i.e.*, the contribution to the total flux that is driven by the gradient of electrostatic potential, see eq 13 in Methods) is higher for the low-resistance entrance reservoir than for the high-resistance exit one. As a consequence of the imbalance of migration fluxes in both reservoirs, cations accumulate inside the pore. The increased cation concentration inside the pore creates a diffusion flux (*i.e.*, the component of the total flux driven by concentration gradients) into the upper reservoir that balances the migration flux and a nonequilibrium steady state is established.

The argument discussed above for the cations can be applied to the anions (inverting both the direction of flow and the resistances of the reservoirs), and therefore, the concentration of both cations and anions is enhanced within the pore in the *on* state. In the *off* state, the entrance resistance for both cations and anions is higher than the exit resistance and therefore both anions and cations are depleted from the pore.

An Analytical Model for the Current Response of Neutral Nanopores with Charged Outer Walls. We derived a simplified analytical model to explain ion conductivity in nanopores with chemically modified (surface-charged) outer walls by solving the Poisson−Nernst−Planck (PNP) equations approximately. The model is derived in detail in the Supporting Information. The applied potential ΔV required to generate a current I predicted by the model is

$$\Delta V = \frac{I}{2}\left(\frac{\Omega^{\text{pore}}}{1-\frac{I}{2}(\Omega^{=}-\Omega^{\neq})\beta|e|}+\Omega^{=}+\Omega^{\neq}\right) \quad (1)$$

where Ω^{i} are electrical resistances for the flux of one type of ions (*i.e.*, the electrical resistance to the flux of cations or anions) at zero applied bias (*i.e.*, these resistances can be determined from equilibrium considerations). More specifically, $\Omega^{=}$ and $\Omega^{\neq}$ are the resistances of the reservoirs for the flux of an ion with a charge of equal or opposite sign than the charges on the outer walls of the reservoir, respectively, and Ω^{pore} is the equilibrium resistance of the pore. Note that eq 1 differs from Ohm's law for a system close to the equilibrium by the factor dividing Ω^{pore}; this factor accounts for the changes in salt concentration within the pore under nonequilibrium conditions. In other words, the potential-bias-dependent salt concentration inside the pore is

$$c^{\text{pore}} = c^{\text{bulk}}\left(1-\frac{I}{2}(\Omega^{=}-\Omega^{\neq})\beta|e|\right) \quad (2)$$

The resistances in eq 1 can be calculated from the following expressions (see Supporting Information):

$$\Omega^{\text{pore}} = \frac{L}{\pi R^2 D c^{\text{bulk}}\beta|e|^2}+\frac{1}{RDc^{\text{bulk}}\beta|e|^2}\left(\frac{1}{2}-\frac{1}{\pi}\right) \quad (3)$$

$$\Omega^{=} = (2\pi D c^{\text{bulk}}\beta|e|^2 R)^{-1} \quad (4)$$

$$\Omega^{\neq} = \Omega^{=}\frac{\ln\left(1+\frac{\sigma_q}{Rc^{\text{bulk}}}\right)}{\frac{\sigma_q}{Rc^{\text{bulk}}}} \quad (5)$$

where D is the ions diffusion coefficient (in this work, we assume D to be the same for anions and cations in all parts of the system), c^{bulk} is the bulk salt concentration, $\beta = 1/k_B T$ and $|e|$ is the absolute value of the elemental charge. In eq 3, Ω^{pore} is the combination of two terms: the first term describes the resistance of the pore itself and the second term is the resistance of the hemispheres located at the entrances of the pore. A careful analysis of these equations reveals that, as expected, $\Omega^{=} > \Omega^{\neq}$. In the limit of neutral outer walls ($\sigma_q \to 0$, more specifically $\sigma_q \ll Rc^{\text{bulk}}$), $\Omega^{=}$ and $\Omega^{\neq}$ become equal and eq 1 becomes linear (Ohm's law), with a total resistance $(\Omega^{=}+\Omega^{\neq}+\Omega^{\text{pore}})/2$ (the factor 1/2 in this expression is due to the fact that the Ω^{i} are electrical resistances for one type of ions only). The current can be isolated from eq 1 as

$$I = [(\beta|e|\Delta V\Omega^{-}+\Omega^{\text{pore}}+\Omega^{+}) - ((\beta|e|\Delta V\Omega^{-}+\Omega^{\text{pore}}+\Omega^{+})^2 - 4\beta|e|\Delta V\Omega^{-}\Omega^{+})^{1/2}]/\beta|e|\Omega^{-}\Omega^{+} \quad (6)$$

where we defined $\Omega^{+} = \Omega^{=} + \Omega^{\neq}$ and $\Omega^{-} = \Omega^{=} - \Omega^{\neq}$ for convenience. Using eq 6, the current rectification factor for a given $|\Delta V|$ is

$$\alpha(|\Delta V|) = -I(-\Delta V)/I(\Delta V) = [\beta|e||\Delta V|\Omega^{-} - (\Omega^{\text{pore}}+\Omega^{+}) + ((\beta|e||\Delta V|\Omega^{-} - (\Omega^{\text{pore}}+\Omega^{+}))^2 + 4\beta|e||\Delta V|\Omega^{-}\Omega^{+})^{1/2}]/[\beta|e||\Delta V|\Omega^{-}+(\Omega^{\text{pore}}+\Omega^{+}) - ((\beta|e||\Delta V|\Omega^{-}+(\Omega^{\text{pore}}+\Omega^{+}))^2 - 4\beta|e||\Delta V|\Omega^{-}\Omega^{+})^{1/2}] \quad (7)$$

Figures 2 and 3 show very good agreement between analytical predictions (solid lines) and numerical

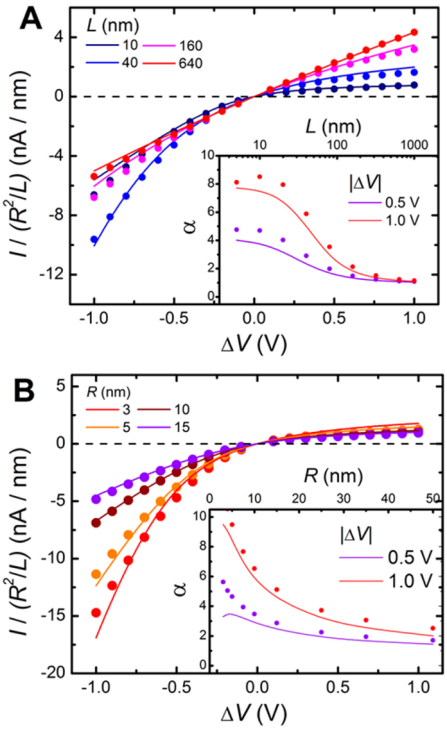

Figure 4. Current−potential plots for nanopores with surface-charged outer walls for different pore lengths, *L* (A) and radii, *R* (B). The current has been normalized by the factor R^2/L. Insets: Rectification factor α as a function of *L* (A) and *R* (B). Solid symbols show the results of the numerical solution of the nonequilibrium molecular theory; lines show the predictions of the analytical model. Same calculation parameters as in Figure 2 (with exception of *L* in (A) and *R* in (B)).

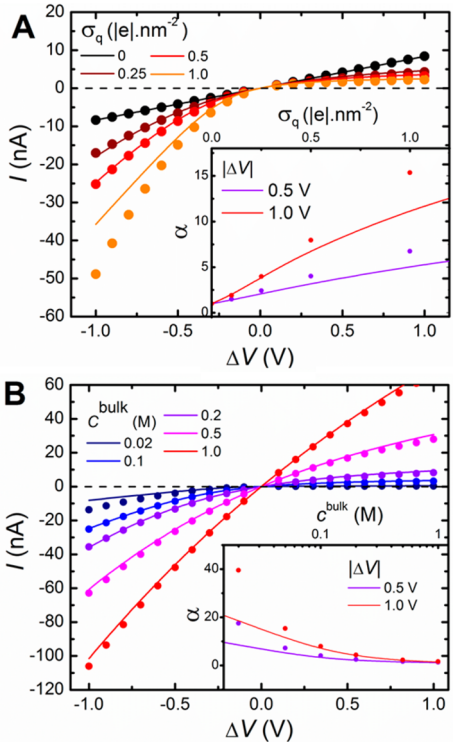

Figure 5. Current−potential plots for nanopores with surface-charged outer walls for different surface charge densities, σ_q (A) and bulk salt concentration, c^{bulk} (B). Insets: Rectification factor α as a function of σ_q (A) and bulk salt concentration, c^{bulk} (B). Solid symbols show the predictions of the nonequilibrium molecular theory; lines show the predictions of the analytical model. Same calculation parameters as in Figure 2 (with exception of σ_q in (A) and c^{bulk} in (B)).

calculations (symbols) for a current−potential curve and the potential-dependent salt concentration inside the pore, respectively. We will show in the next sections that the predictions of the analytical model are also in very good agreement with numerical simulations for different combinations of system parameters (Figures 4 and 5 in the next section).

Effect of System Parameters on the Ion-Current Response of Neutral Nanopores with Surface-Charged Outer Walls. In this section, we study how current rectification depends on the parameters of the system. Before presenting the results from numerical calculations, it is instructive to consider the different length and energy scales in the problem and analyze their competition. Dividing eqs 3 by 4 reveals that $\Omega^{pore}/\Omega^{=} \propto L/R$, and therefore, the competition between pore length and radius determines the relative contribution of the pore and reservoir resistances to the total resistance. Inspection of eq 5 shows that $\Omega^{\neq} \rightarrow \Omega^{=}$ when $R \gg \sigma_q/c^{bulk}$ (see Supporting Information); therefore σ_q/c^{bulk} is a very important length scale in the system. This length scale is the thickness of a solution layer that has a number of counterions per unit area equal to σ_q. For a given type of ions (cations or anions), we defined $\Omega^{\neq}$ as the resistance of the reservoir with outer walls bearing charges of opposite sign to that of the ion. In this reservoir, the ionic current follows through two parallel pathways: the current through the solution and the surface current (*i.e.*, the current flowing near the surface), see Supporting Information. The surface contribution to the current dominates for $r < \sigma_q/c^{bulk}$ (where *r* is the distance from the pore mouth), while for $r > \sigma_q/c^{bulk}$, the main contribution to the total current is the current through the solution. Therefore, when σ_q/c^{bulk} is similar to or larger than *R* (the pore radius), the large concentration of charge carriers in the surface layer near the (oppositely charged) membrane increases the conductivity *via* the surface current mechanism and $\Omega^{\neq}$ is smaller than the resistance of the reservoir bearing charges of the same sign as the ion ($\Omega^{=}$). The length scale σ_q/c^{bulk} dictates, therefore, the difference between the access and exit resistances.

In addition to the three length scales discussed above (*L*, *R* and σ_q/c^{bulk}), there are two relevant energy scales: the thermal energy ($k_BT = \beta^{-1}$) and the electrostatic energy ($|\Delta V||e|$). The competition between these energy scales is given by the factor $\beta|\Delta V||e|$, which appears in eqs 6 and 7. The factor $\beta|\Delta V||e|$ determines whether the applied potential is high enough to produce changes in the salt concentration within the pore; therefore, the current−potential curves are always linear (ohmic) for $|\Delta V| \ll \beta^{-1}|e|^{-1}$

(with $\beta^{-1}|e|^{-1}$ = 25 mV), while for $|\Delta V| \gg \beta^{-1}|e|^{-1}$, current rectification is predicted.

We analyze in Figure 4 the effect of pore length (panel A) and pore radius (panel B) on the current−potential curves; the symbols in the figure are numerical results and the solid lines are predictions from the analytical model, eqs 6 and 7. To better appreciate the shape of the current−potential curves shown in Figure 4, we have scaled the currents by a factor R^2/L, which is proportional to the conductance of a long nanochannel.[32,33]

Figure 4A shows that the rectification factor α decreases with increasing pore length. Let us consider pores with $L \gg R$, where Ω^+ and Ω^- are much smaller than Ω^{pore}. Under these conditions, we can derive the following approximate expression (see Supporting Information):

$$\alpha(|\Delta V|) = \frac{1 + \frac{\Omega^-}{\Omega^{pore}}\beta|\Delta V||e|}{1 - \frac{\Omega^-}{\Omega^{pore}}\beta|\Delta V||e|} \quad (8)$$

Equation 8 reveals that current rectification increases when the factor $\beta|\Delta V||e| \cdot \Omega^-/\Omega^{pore}$ increases. This factor combines the competition between the thermal and electrostatic potential energies discussed above (given by $\beta|e||\Delta V|$) and the factor Ω^-/Ω^{pore}. The latter ratio represents the competition between the driving force for rectification (given by Ω^-, the difference of the resistances of the two reservoirs) and the total resistance (which, in the limit of long pores, is given by the resistance of pore). In the long-pore regime, Ω^-/Ω^{pore} is proportional to R/L, which means that the rectification efficiency decays as the pore length increases. This result is expected because the influence of the reservoirs diminishes as the pore length increases. Note, however, that large rectification factors can be achieved even for long pores providing that a large enough ΔV is applied (*i.e.*, $\Delta V > \beta^{-1}|e|^{-1} \cdot \Omega^{pore}/\Omega^-$), for example, the theory predicts α = 7.8 for a 0.5-μm long pore and $|\Delta V|$ = 10 V (current breakdown was not observed for the system and potential range under study, see Figure S5 in the Supporting Information). In the limit of short pores, $L < R$, the total resistance of the system is dominated by the resistance of the reservoirs, which is independent of the applied potential; therefore, as L decreases, α tends to a constant value (see inset of Figure 4A).

Figure 4B shows that α decreases with increasing pore radius. As we discussed above, the imbalance between exit and entrances resistances, which determines current rectification, depends on the competition between R and σ_q/c^{bulk} (for the conditions of Figure 4B, σ_q/c^{bulk} = 8.3 nm). Therefore, the current rectification factor decreases with increasing Rc^{bulk}/σ_q. Moreover, for wide pores, the relative contribution of the pore resistance to the total (pore + reservoirs) resistance is smaller than that for narrow pores (see competition between L and R above). Since the resistance of the reservoirs is independent of the applied potential, this effect also contributes to the decrease of α with increasing R predicted in Figure 4B.

In panels A and B of Figures 5, we show that the current rectification factor increases for increasing σ_q (charge density on the outer walls) or decreasing c^{bulk} (bulk salt concentration), respectively. These effects can be explained by the competition between the length scales R and σ_q/c^{bulk}, discussed above. Increasing σ_q or decreasing c^{bulk} increases the characteristic length scale of the influence of the charges on the outer walls and, therefore, increases the imbalance between access and exit resistances that causes current rectification.

The analytical model given by eqs 6 and 7 is in good agreement with the numerical calculations for different values of L, R, c^{bulk} and σ_q, although the analytical model always underestimates the rectification efficiency. More specifically, the analytical model underestimates the current in the *on* state and overestimates that in the *off* state. The discrepancies are largest for low salt concentrations and highly charged walls. We attribute the error in the analytical model to the underestimation of $\Omega^=$ (the resistance for the flow of an ion through the reservoir with surface charges of the same sign), since in the analytical model we estimate $\Omega^=$ to be equal to the resistance of a neutral reservoir, while in reality it should be larger than that due to the unfavorable electrostatic interactions of the translocating ion with the outer walls of the same charge. The magnitude of the error will increase as the strength of the electrostatic interactions increases, *i.e.*, increasing charge density or decreasing salt concentration.

Alternative Pore Designs: Effects of Nanopore Shape and Charge Distribution on Current Rectification. In previous sections, we discussed current rectification for cylindrical nanopores with charged outer walls and neutral inner walls. In this section, we consider different pore shapes and charge distributions. Figure 6 shows the different scenarios under theoretical investigation and the rectification factor of the pores for $|\Delta V|$ = 1 V. For comparison, we included in Figure 6A,B cylindrical nanopores with neutral inner walls and charged outer walls (*i.e.*, the nanopore design studied so far). The 10-nm cylindrical pore (panel A, α = 9.5) is a better rectifier than the 15-nm pore (panel B, α = 7.7), in agreement with the predicted effect of R on α (results in Figure 4B).

Membrane materials used in solid state membranes, such as Si_3N_4 and SiO_2 have a non-zero intrinsic surface charge density.[39−41] Therefore, we have studied the effect of the charge density of the inner surface of the pore on the efficiency of rectification. Our calculations show that the rectification factor increases for increasing charge density of the inner walls, but the magnitude of the effect is small. For example, we predict α(|1 V|) = 8.1 for a 15-nm cylindrical

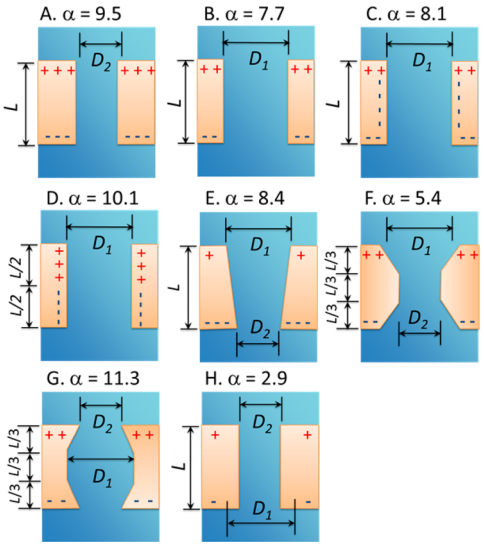

Figure 6. Schemes of different pore shapes and surface charge distributions under study: (A) 10-nm cylindrical pore; (B) 15-nm cylindrical pore; (C) 15-nm cylindrical pore with negatively charged inner walls; (D) cylindrical pore with neutral outer walls and bipolar inner walls; (E) conical pore; (F) semi-biconical pore; (G) inverted semi-biconical pore; (H) 15-nm cylindrical pore with a neutral region at the edges. The rectification factor α for $|\Delta V| = 1$ V for each pore is shown above the corresponding scheme. Calculation parameters: $D_1 = 15$ nm, $D_2 = 10$ nm, $L = 20$ nm. All charged surfaces (including inner walls in systems C and D) have a charge density of ± 0.5 $|e|\cdot nm^{-2}$. Other parameters were the same as in Figure 2.

nanopore with inner walls bearing a charge density of -0.5 $|e|\cdot nm^{-2}$ (Figure 6C), which should be compared to $\alpha(|1\ V|) = 7.7$ for a 15-nm cylindrical nanopore with neutral inner walls (Figure 6B). In Figure S7 of the Supporting Information, we present a systematic study of the effect of the charge density of the inner walls on current rectification.

In Figure 6D, we consider the bipolar diode design previously studied by Vlassiouk *et al.*[31] and Daiguji *et al.*[4] The rectification efficiency predicted for the pore with bipolar inner walls (α = 10.1, panel D) is larger than that predicted for the nanopore of the same diameter with charged outer walls and neutral inner walls (α = 7.7, panel B). This difference will increase for pores longer than those in Figure 6 because α increases with *L* for the pore with bipolar inner walls,[31] but it decreases with *L* for the pore with bipolar outer walls considered here. We believe that the main advantage of the pore with bipolar outer walls over that with bipolar inner walls resides in its preparation: imparting the bipolar charge configuration could be easier experimentally for outer walls than for the inner walls, for example, by introducing opposite charges on both sides of the membrane before drilling the nanopore.

Solid-states nanopores drilled in ultrathin membranes have geometries that may depart from ideal cylindrical pores,[34,39] and therefore, we would like to know how the shape of the pore influences current rectification. A conical pore (Figure 6E) with pore entrances of 10 and 15 nm in diameter has a rectification efficiency of 8.4, which is between those of the 10- and 15-nm cylindrical nanopores (panels A and B, α = 9.5 and 7.7, respectively). A semi-biconical nanopore with an outer diameter of 15 nm and an inner diameter of 10 nm (Figure 6F) has a rectification efficiency of α = 5.4, which is smaller than those of the 15- and 10-nm cylindrical pores. On the other hand, an inverted semi-biconical pore (Figure 6G) has a rectification factor α = 11.3, which is larger than those of the cylindrical pores. We can explain these observations by recalling that the rectification factor depends approximately on the ratio Ω^-/Ω^{pore} (see discussion of eq 8). In the semi-biconical case, the inner part of the pore is 10 nm wide, so Ω^{pore} will be larger than the corresponding Ω^{pore} for the 15-nm cylindrical pore (both Ω^{pore} and Ω^- increase for decreasing pore radius). On the other hand, the entrances of the semi-biconical pore are 15 nm wide and thus its Ω^- will be similar to that of a 15-nm cylindrical pore. Therefore, the semi-biconical pore has Ω^-/Ω^{pore} and α smaller than the 15-nm cylindrical pore. The same argument can be applied to the inverted semi-biconical pore: in this case, Ω^- will be similar to that of the 10-nm cylindrical pore and Ω^{pore} will be smaller than that for the 10-nm cylindrical case; therefore, the inverted semi-biconical pore will exhibit a higher rectification than the 10-nm cylindrical pore.

In panel H of Figure 6, we studied the effect of having a neutral zone between the edge of the pore and the charged region. This scenario presents a rectification factor of α = 2.9, which is much smaller than the value of α = 9.5 predicted for the nanopore of the same diameter without the neutral region at the edge of the pore (panel A). Moreover, increasing the thickness of the neutral region decreases the rectification efficiency rapidly (see Supporting Information, Figure S8).

Finally, we investigated the effect of having different charge densities on the outer membranes. For a constant sum of the absolute values of the charge densities on the upper and inner membranes, the rectification efficiency is maximal when the membranes are charged symmetrically (*i.e.*, the charge density has the same absolute value on each side of the membrane); see Figure S9 in the Supporting Information.

Current Rectification in Neutral Nanopores with Polyelectrolyte-Modified Outer Walls. In recent years, the surface modification of nanofluidic devices with polyelectrolyte brushes has attracted much attention.[15,20,22,32,33,42−44] An important advantage of polyelectrolyte brushes compared to surface charges is that the density of charges per unit area can be increased by using longer polyelectrolyte chains. Figure 7A compares the current−potential curves for neutral nanopores with outer walls modified by polyelectrolyte brushes of different chain lengths (*N*) and a constant surface density of $\sigma_{pol} = 0.15$ chains·nm^{-2}

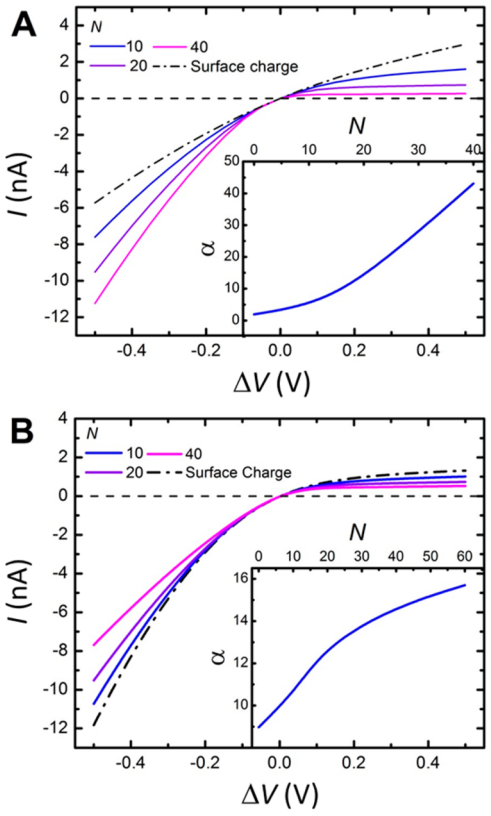

Figure 7. Current–potential plots for nanopores with polyelectrolyte-modified outer walls for different chain lengths, *N*, predicted by the nonequilibrium molecular theory. Curves for the surface-charged system are shown as dash-dotted lines for comparison. Insets: Rectification factor α as a function of *N* for $|\Delta V| = 0.5$ V. Panel A shows results for a constant polyelectrolyte grafting density $\sigma_{pol} = 0.15$ chains·nm^{-2} ($\sigma_q = 0.15$ $|e|\cdot$nm^{-2} for the surface-charged outer walls). Panel B shows calculations for constant total surface charge density $N\sigma_{pol}f = 1.0$ $|e|\cdot$nm^{-2} ($\sigma_q = 1.0$ $|e|\cdot$nm^{-2} for the surface-charged outer walls).

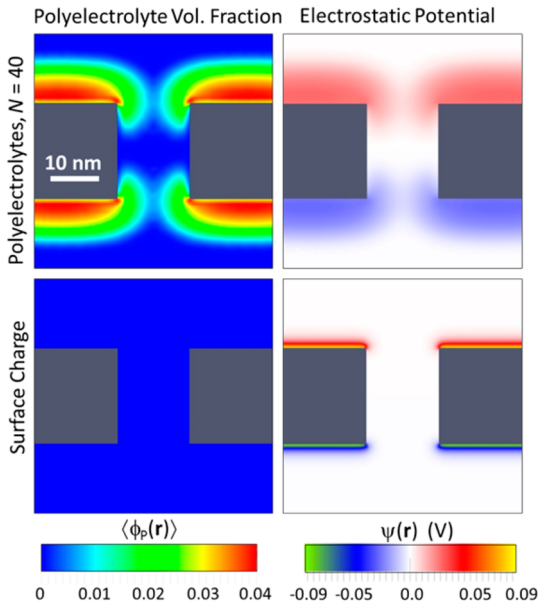

Figure 8. Color maps of polyelectrolyte volume fraction (left) and electrostatic potential (right) for pores with polyelectrolyte-modified outer walls (top) and surface-charged outer walls (bottom). The calculations correspond to equilibrium conditions ($\Delta V = 0$). The density of charges in the pore with surface-charged outer walls is $\sigma_q = 1.0$ $|e|\cdot$nm^{-2}. The polyelectrolyte chains in the polyelectrolyte-modified outer walls pore have $N = 40$ and $\sigma_{pol} = 0.075$ chains·nm^{-2} (thus the total surface charge density is the same for both systems: $\sigma_q = N\sigma_{pol}f = 1.0$ $|e|\cdot$nm^{-2}). Other calculation parameters were the same as in Figure 2.

(which is typical for "grafted-from" polyelectrolyte brushes[45]). We make in this work the conservative assumption that only one-third of the segments are charged (charge per monomer, $f = 1/3|e|$), thus the total charge density is $N\sigma_{pol}/3$. For comparison, we also included in Figure 7A the current–potential trace predicted for a surface-charged system with $\sigma_q = 0.15$ $|e|\cdot$nm^{-2}. Our theory predicts that for increasing *N*, the current in the *on* state increases and the current in the *off* state decreases. As a consequence, the rectification efficiency increases with *N* and reaches a value of $\alpha = 42$ for $N = 40$ (for $|\Delta V| = 0.5$ V) ; this rectification efficiency is comparable to that obtained or predicted for highly rectifying nanopores, such as conical nanopores[19,22] and bipolar diodes[26,31] for similar applied biases and bulk electrolyte concentration.

We have shown in Figure 5A that α increases linearly with σ_q (the charge density for the surface-charged case), which suggests that the high rectification efficiency obtained for nanopores with $N = 40$ may be mainly the result of the very large charge density, $N\sigma_{pol}f = 2.0$ $|e|\cdot$nm^{-2}. To isolate the effect of chain length from that of surface charge density, we varied *N* and σ_{pol} simultaneously in order to keep a constant charge density on the outer walls; *i.e.*, we fixed the product $N\sigma_{pol}f$ to 1.0 $|e|\cdot$nm^{-2}. Figure 7B shows that α increases with *N* even when $N\sigma_{pol}f$ is held constant and, for $|\Delta V| = 0.5$ V, α is 2.6 times larger for the polyelectrolyte-modified outer walls with $N = 40$ than for the surface-charged case. The result in Figure 7B shows that the length of the polyelectrolyte chain is an important length scale for nanopores with polyelectrolyte-modified outer walls, which is absent in the surface-charged system.

To understand how the length of the polyelectrolyte chains affects current rectification, we compare in Figure 8 the equilibrium polymer density and electrostatic potential for pores with outer walls modified by polyelectrolyte brushes ($N = 40$, upper panels) and surface charges (bottom panels). In these calculations, the total charge density for the surface-charged and polyelectrolyte-modified cases is the same (1.0 $|e|\cdot$nm^{-2}) in order to separate the effect of chain length from that of charge density. In the case of surface-charged outer walls, we observe that the electrostatic potential is very strong close to the walls but decays within a few nanometers (*i.e.*, a few Debye lengths). In the polyelectrolyte-modified system, the polyelectrolyte chains extend ~8 nm from the walls and explore the interior of the pore. Long chains extend into the pore in order

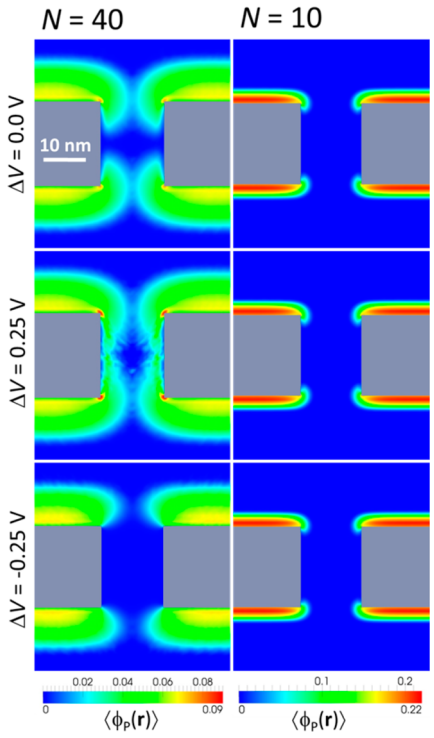

Figure 9. Color maps of polyelectrolyte volume fraction for pores with polyelectrolyte-modified outer walls and different applied biases for $N = 40$, $\sigma_{pol} = 0.15$ chains·nm^{-2} (right panels) and $N = 10$, $\sigma_{pol} = 0.6$ chains·nm^{-2} (left panels). Note that N and σ_{pol} are chosen such that the total charge density $f\sigma_{pol}N = 2.0$ $|e|$·nm^{-2} in both cases. Other calculation parameters were the same as in Figure 2.

to increase their conformational entropy, reduce the osmotic pressure within the layer and minimize the electrostatic repulsions between charged segments.[46,47] The electrostatic potential in the polyelectrolyte-modified case follows the distribution of the polymer. The presence of charged segments within the pore enhances the imbalance between entrance and exit resistances and thus increases the current rectification factor. The effect of having charged segments inside the pore is qualitatively equivalent to decreasing the radius and length of the pore. In summary, the pore with polyelectrolyte-modified outer walls is a better rectifier than the surface-charged case due to the combination of two effects: (i) polyelectrolyte brushes allow to immobilize larger charge densities than surface charges and (ii) the conformational flexibility of polyelectrolyte brushes places charged segments in the interior of the pore.

Transport Gating in Neutral Nanopores with Polyelectrolyte-Modified Outer Walls. In Figure 9, we show the effect of the applied bias on the total distribution of polyelectrolyte segments for $N = 40$ (left panels) and $N = 10$ (right panels). For $N = 40$, the polyelectrolyte chains on the outer walls respond to the applied potential by stretching in the direction of the oppositely charged electrode. Because of this process, the polyelectrolyte chains block the pore for $\Delta V = 0.25$ V (middle panel) and form a polyelectrolyte-free channel for $\Delta V = -0.25$ V (bottom panel). As we discussed in our previous work,[32] the deformation of the polyelectrolyte layers arises from the presence of the electric field within the pore, which is sustained by the ionic currents. The $N = 40$ system depicted in the left panels of Figure 9 behaves, therefore, as an electromechanical gate, whose *open* and *closed* states coincide with the *on* and *off* ion-conductivity states. The polyelectrolyte layer for the $N = 10$ system (shown in the right panels of Figure 9) is almost unaffected by the applied bias due to the small conformational flexibility of the short polyelectrolyte chains.

It is interesting to consider the transport of a cargo larger than an ion through the nanopores depicted in Figure 9. The translocation of such cargo will be strongly influenced by the conformations of the polyelectrolyte chains and, therefore, the applied potential. To explore this idea, we studied the translocation of charged cargoes by calculating their potential of mean force (pmf) along the z-coordinate. The pmf at position $\mathbf{r}$ is the work required to bring the cargo from the bulk solution (we choose the lower reservoir as the reference bulk solution) to $\mathbf{r}$, *i.e.*, it is the nonideal part of the chemical potential of the particle.[48] For a test particle, the pmf is[49]

$$U^{pmf}(\mathbf{r}) = \int_V (\pi(\mathbf{r}') - \pi^{bulk,\,lower}) v_{cargo}(\mathbf{r}, \mathbf{r}') d\mathbf{r}' + \int_V (\psi(\mathbf{r}') - \psi^{bulk,\,lower}) q_{cargo}(\mathbf{r}, \mathbf{r}') d\mathbf{r}' \quad (9)$$

where $\pi(\mathbf{r})$ and $\psi(\mathbf{r})$ are the osmotic pressure and the electrostatic potential at $\mathbf{r}$ determined from the numerical solution of the molecular theory in the absence of the test cargo, $v_{cargo}(\mathbf{r}, \mathbf{r}')$ and $q_{cargo}(\mathbf{r}, \mathbf{r}')$ are the volume and charge that a cargo with its center at $\mathbf{r}$ has in the volume element between $\mathbf{r}'$ and $\mathbf{r}' + d\mathbf{r}'$ and the integrals run over the total volume of the cargo. It is important to mention the approximations involved behind eq 9: (i) Our method to determine the pmf neglects the perturbations introduced by the presence of the particle, such as its influence on the ion currents or the particle-induced deformation of the polyelectrolyte layer.[47] The quality of this approximation will be better for small and low-charged cargoes than for large and highly charged ones, because the former perturb the system much less than the latter. (ii) The pmf is an equilibrium quantity, while our system is out of equilibrium. It is therefore necessary to assume that the time scale of the motion of the cargo is much slower than that of the small ions. (iii) The pmf calculation neglects nonequilibrium forces such as electroosmotic drag; however, in our system, cation and anion currents are of equal magnitude but opposite direction, and therefore, the velocity of the solution is expected to be close to zero inside the pore.[31] Despite these approximations, the pmf serves as a criterion to determine whether the particle can translocate through the

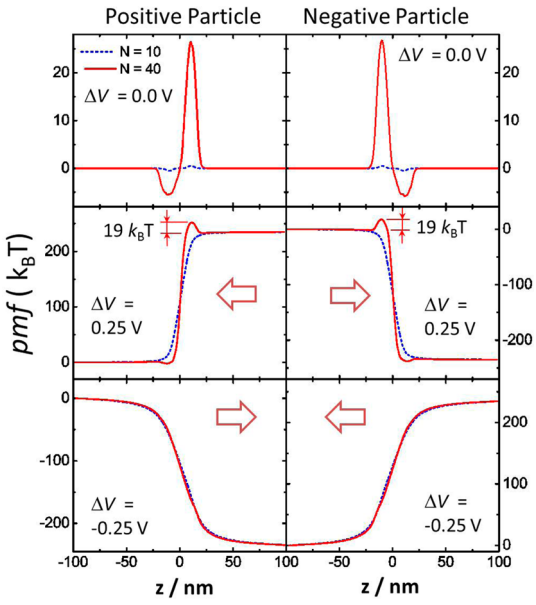

Figure 10. Potential of mean force as a function of position for the translocation of a particle along the axis of the nanopores shown in Figure 9, for $\Delta V = 0$ (top panels), 0.25 (middle panels), and −0.25 V (lower panels). The particle has a radius of 1.5 nm and a charge of $+24|e|$ (left panels) or $-24|e|$ (right panels). The arrows show the direction of translocation. The heights of the free energy barriers for particle translocation for $\Delta V = 0.25$ V are shown explicitly. The outer walls of the membrane are located at $z = -10$ (negatively charged polyelectrolyte brush) and $z = 10$ nm (positively charged polyelectrolyte brush).

pore: the presence of an energy barrier much larger than the available thermal energy (k_BT) would likely result in an inability of the cargo to translocate the pore.

Figure 10 shows the pmf for the translocation of a particle of radius 1.5 nm, bearing either $+24|e|$ or $-24|e|$ charges (which we homogeneously distribute over the volume of the particle), for the systems shown in Figure 9. It is worthwhile to recall that in these systems we fixed the total density of charges on the outer walls to $N\sigma_{Pol}f = 2.0\ |e|\cdot nm^{-2}$ in order to separate the effect of chain length from that of charge density (we used $\sigma_{pol} = 0.15$ chains$\cdot nm^{-2}$ for $N = 40$ and $\sigma_{pol} = 0.6$ chains$\cdot nm^{-2}$ for $N = 10$). The upper panels in Figure 10 show that the pmf for the translocation of positive (right panel) and negative (left panel) particles at $\Delta V = 0$ V present potential barriers for translocation. As expected, these barriers are located at the position of the outer walls bearing the same charge as the translocating particle. The pmf have also potential wells at the position of the outer walls of opposite charge that the particle. The barriers are larger for $N = 40$ (26.5 k_BT) than for $N = 10$ (0.5 k_BT) because long chains can reach the axis of the pore, while the short ones cannot (see Figure 9). It is interesting to observe that for $N = 40$ the height of the barriers is larger than the depth of the wells. The reason for this asymmetry is that the pmf has both steric and electrostatic components. The electrostatic attractions and repulsions are equal in magnitude, but the steric interactions are always repulsive, and therefore, they break the symmetry between barriers and wells. For $N = 10$ this asymmetry is less marked than for $N = 40$, because the steric interaction is very small due to the fact that the short polyelectrolyte chains do not reach the position of the translocating particle.

In nonequilibrium conditions (middle and lower panels in Figure 10), the potentials of mean force have different values in the two reservoirs due to the applied potential. Note that the applied potential results in a very large thermodynamic driving force for translocation (234 k_BT for $\Delta V = \pm 0.25$ V); however, the kinetics of particle translocation will be dictated by the presence of barriers in the pmf: a barrier much larger than k_BT will prevent the particle to translocate the pore. The arrows in the middle and lower panels in Figure 10 indicate the direction of translocation for the negative and positive charged cargoes. For $\Delta V = 0.25$ V (middle panels), the pmf show a barrier of ~19 k_BT for $N = 40$ and no barrier for $N = 10$ for both positive and negative particles. In other words, the translocation barriers at 0.25 V are lowered slightly with respect to the equilibrium ones due to the applied potential; however, for $N = 40$, these barriers are still high enough to prevent the translocation of the cargoes. On the other hand, for $\Delta V = -0.25$ V, the barriers for translocation disappear for all different combinations of particle charge and polyelectrolyte chain length. This result is consistent with the results in Figure 9 where the polyelectrolyte chains retract from the pore for negative applied biases, leaving an open channel for the particles to cross. To conclude, the translocation of large particles through the pore can be switched on and off by the potential-induced reorganization of long polyelectrolyte chains (but not by that of short ones). Both positive and negative particles can translocate for $\Delta V < 0$ V (which corresponds to the *on* current state for the ions) and are blocked for $\Delta V \geq 0$ V (the *off* current state).

CONCLUSIONS

We presented a detailed study of transport in cylindrical nanopores with chemically modified outer walls and demonstrated their current-rectifying properties. We used in our analysis a previously developed molecular theory[32] that considers the organization of the system at the mean-field level and the nonequilibrium fluxes with a generalized diffusion approach. This type of molecular theories allows including molecular information when studying problems that, due to their dimensions and long time scales, are very costly (if ever possible) to simulate with atomistic detail. Our theory has two main advantages over the PNP equations that are typically used to study ion currents in nanopores and nanochannels: (i) The theory considers explicitly the size, shape and conformations of all molecular species in the system, most notably the presence and stimuli responsiveness of polyelectrolyte-grafted chains. Moreover, the theory can

be extended to other macromolecular species besides polyelectrolyte brushes, such as gels,[50] adsorbed polyelectrolyte layers[51] and lipids.[52] (ii) The theory explicitly includes the electrostatic and nonelectrostatic interactions among all the species; for example, it considers steric repulsive interactions, which are neglected in the PNP approach. Despite these advantages, some approximations are required: (a) We neglect electroosmotic flows in the system. The contribution of electroosmosis to the total current is expected to be negligible in the present case because the cation and anion currents inside the pore have equal magnitude and are of opposite direction.[31] (b) Our theory is a mean-field theory, and therefore, it neglects correlations in the system, such as ion-pairing between the polyelectrolytes and their counterions. (c) The diffusion coefficients of the ions are assumed to be constant across the system and equal to their bulk values; this approximation is justified by the high solvent content of the polyelectrolyte layers. For simplicity, we also neglected the charge regulation of polyelectrolyte chains in the present work, but we plan to address the conductivity of short nanopores modified by pH-responsive layers in the future.

The nanopore design studied in this work presents some interesting differences with other rectifying nanopores, such as bipolar diodes (where the inner walls have charges of opposite sign in the upper and lower halves of the pore) and charged conical nanopores. For instance, we showed that the rectification factor in our system decreases for increasing pore length, while the opposite behavior is expected for bipolar diodes[51] and conical nanopores.[53] Therefore, the nanopores discussed in this work can be experimentally implemented in thin membranes (such as solid-state membranes[30,31,54]), rather than thick ones (*e.g.*, ion-track etched membranes[55]). While fabrication of bipolar diodes requires precise composition control of the inaccessible inner walls, the preparation of the nanopores discussed in this work would require modification of the outer walls only, which may be accomplished before drilling the pore. In such experiment, the elimination of charged species close to the edge of the pore should be avoided, since we have shown that neutralizing the charges within a few nanometers from the pore edge degrades the efficiency of rectification.

We have introduced a simple model based on an approximate solution of the PNP equations that agrees well with numerical predictions for moderate surface charges and ionic strengths. It is worthwhile to mention that the analytical model cannot be applied to the polyelectrolyte-modified case due to the complexity of the structure of the polyelectrolyte layer and its reorganization with the applied potential. Nowadays, it is possible to calculate the current response of nanopores and nanochannels at the PNP level of theory using commercially available computer codes; however, analytical models are important for two reasons. First, they provide physical insights in a simple form and allow understanding the physics of the problem and the general trends in terms of the competition between length and energy scales, without the need of scanning through system parameters using numerical calculations. Second, we envision that as we move from single nanopores to integrated nanopore networks[56,57] the size of these networks will limit numerical analysis, and thus, analytical models will be required. Several analytical models have been proposed in the literature for bipolar diodes and conical nanopores.[4,21,23,51] The major differences between these models and that presented here are (i) we consider explicitly the resistance of the reservoirs (which is key to understand current rectification in our system), while models for long pores usually neglect this contribution and (ii) the $I-V$ relation in our model can be expressed in terms of the combination of the electrical resistances of the different parts of the system for a given type of ion; this form of the equation facilitates the physical interpretation of the model and provides a potential route to extend it to other nanopore designs.

Modification of nanopore outer walls with polyelectrolyte chains is predicted to produce high rectification factors. Moreover, we proposed that nanopores with outer walls modified by long polyelectrolyte chains rectify not only fluxes of ions, but also the translocation of large molecules. This ability is originated in the deformation of the polyelectrolyte layer with the applied potential, which behaves as an electromechanical gate. Rectifying the transport of biomolecules, such as proteins or DNA fragments, can be especially attractive for applications in biosensing and separation. Nanopores with polyelectrolyte-modified outer walls emerge from this work as a promising new type of nanofluidic elements with diode-like current behavior and potential-driven actuation.

METHODS

Our predictions are based on a steady-state molecular theory; we refer the reader to our previous work[32] and the Supporting Information for the details of the derivation and implementation of the theory. Briefly, the theory follows the ideas of the local equilibrium approximation,[58,59] which assume that thermodynamic variables are defined locally and related by the same functional forms as in equilibrium. In the theory, the fluxes of ions are driven by the respective gradients of chemical potential.

$$\mathbf{J}_i(\mathbf{r}) = -D_i\rho_i(\mathbf{r})\nabla\beta\mu_i(\mathbf{r}) \quad (10)$$

where D_i, $\mu_i(\mathbf{r})$ and $\rho_i(\mathbf{r})$ are the diffusion coefficient, position-dependent chemical potential, and position-dependent density of the species i, respectively (i = anions and cations). In steady-state, we have

$$\frac{\partial \rho_i(\mathbf{r})}{\partial t} = -\nabla \mathbf{J}_i(\mathbf{r}) = 0 \quad (11)$$

The chemical potential in eq 10 is defined in analogy to the equilibrium one:

$$\beta\mu_i(\mathbf{r}) = \frac{\partial \beta W}{\partial \rho_i(\mathbf{r})} \quad (12)$$

where W is the free energy functional of the system, which follows the expressions developed for equilibrium systems. The different contributions to W (which are discussed in detail in the Supporting Information) are (i) the mixing entropy of water molecules, anions and cations; (ii) the conformational entropy of the polyelectrolyte chains; (iii) the electrostatic energy; and (iv) the energy associated with repulsive interactions, which are modeled as excluded volume interactions. Combination of eqs 10 and 12 yields the following explicit expression for the ion fluxes:

$$\mathbf{J}_i(\mathbf{r}) = -D_i \nabla \rho_i(\mathbf{r}) - D_i \rho_i(\mathbf{r}) q_i \nabla \beta\psi(\mathbf{r}) - D_i \rho_i(\mathbf{r}) v_i \nabla \beta\pi(\mathbf{r}) \quad (13)$$

This equation shows that in the theory the ion fluxes result from the combination of three components: the gradient of ion concentration (first term, known as diffusion flux), the gradient of electrostatic potential (second term, migration flux), and the gradient of osmotic pressure (third term).

The position-dependent electrostatic potential is assumed to respond instantaneously to any change in the system. Therefore, the electrostatic potential is determined as a functional extremum of W, which yields the Poisson equation:

$$\varepsilon \nabla^2 \psi(\mathbf{r}) = -\langle \rho_Q(\mathbf{r}) \rangle \quad (14)$$

Since the polyelectrolyte chains are grafted to the membrane, the probabilities of each chain conformation in the steady state are those that minimize the functional W.

We take advantage of the cylindrical symmetry of the system and assume that the system is homogeneous in the angular coordinate θ, namely, we solve the theory considering inhomogeneities in only two dimensions (r and z). The nonequilibrium molecular theory is solved by numerical methods, as discussed in the Supporting Information.

The molecular theory explicitly accounts for the shape, charge, size, and conformational degrees of freedom of all the species in the system; the relevant inter and intramolecular interactions; and the presence of ion-fluxes. It reduces to the Poisson−Nernst−Planck approximation (which has been widely used to describe ion conductivity in nanopores and nanochannels[11,12,15,17,19,21,23,25,28,31,37,53]) when there are no polyelectrolyte chains in the system and the excluded-volume interactions are neglected, *i.e.*, when not accounting for the size and shape of the ions.

Conflict of Interest: The authors declare no competing financial interest.

Supporting Information Available: Detailed derivation of the nonequilibrium molecular theory and approximate analytical model. Analysis of the effect of the numerical implementation, the size of the reservoirs, the charge distribution on the outer membrane and the dielectric constant on the membrane on the $I-\Delta V$ curves. $I-\Delta V$ curves for an extended potential range. This material is available free of charge *via* the Internet at http://pubs.acs.org.

Acknowledgment. This material is based upon work supported as part of the NERC (Non-Equilibrium Research Center), an Energy Frontier Research Center funded by the U.S. Department of Energy, Office of Science, Office of Basic Energy Sciences under Award Number DE-SC0000989. This research was supported in part through the computational resources and staff contributions provided by the Quest high performance computing facility at Northwestern University which is jointly supported by the Office of the Provost, the Office for Research, and Northwestern University Information Technology. Y.R. would like to acknowledge the support by a grant from the US-Israel Binational Science Foundation.

REFERENCES AND NOTES

1. Cheng, L.-J.; Guo, L. J. Nanofluidic Diodes. *Chem. Soc. Rev.* **2010**, *39*, 923–938.
2. Daiguji, H. Ion Transport in Nanofluidic Channels. *Chem. Soc. Rev.* **2010**, *39*, 901–911.
3. Karnik, R.; Fan, R.; Yue, M.; Li, D.; Yang, P.; Majumdar, A. Electrostatic Control of Ions and Molecules in Nanofluidic Transistors. *Nano Lett.* **2005**, *5*, 943–948.
4. Daiguji, H.; Oka, Y.; Shirono, K. Nanofluidic Diode and Bipolar Transistor. *Nano Lett.* **2005**, *5*, 2274–2280.
5. Siwy, Z.; Trofin, L.; Kohli, P.; Baker, L. A.; Trautmann, C.; Martin, C. R. Protein Biosensors Based on Biofunctionalized Conical Gold Nanotubes. *J. Am. Chem. Soc.* **2005**, *127*, 5000–5001.
6. Ali, M.; Yameen, B.; Neumann, R.; Ensinger, W.; Knoll, W.; Azzaroni, O. Biosensing and Supramolecular Bioconjugation in Single Conical Polymer Nanochannels. Facile Incorporation of Biorecognition Elements into Nanoconfined Geometries. *J. Am. Chem. Soc.* **2008**, *130*, 16351–16357.
7. Sexton, L. T.; Horne, L. P.; Sherrill, S. A.; Bishop, G. W.; Baker, L. A.; Martin, C. R. Resistive-Pulse Studies of Proteins and Protein/Antibody Complexes Using a Conical Nanotube Sensor. *J. Am. Chem. Soc.* **2007**, *129*, 13144–13152.
8. Howorka, S.; Siwy, Z. Nanopore Analytics: Sensing of Single Molecules. *Chem. Soc. Rev.* **2009**, *38*, 2360–2384.
9. Vlassiouk, I.; Kozel, T. R.; Siwy, Z. S. Biosensing with Nanofluidic Diodes. *J. Am. Chem. Soc.* **2009**, *131*, 8211–8220.
10. Sexton, L. T.; Horne, L. P.; Martin, C. R. Developing Synthetic Conical Nanopores for Biosensing Applications. *Mol. BioSyst.* **2007**, *3*, 667–685.
11. Cervera, J.; Ramirez, P.; Mafe, S.; Stroeve, P. Asymmetric Nanopore Rectification for Ion Pumping, Electrical Power Generation, and Information Processing Applications. *Electrochim. Acta* **2011**, *56*, 4504–4511.
12. Ali, M.; Mafe, S.; Ramirez, P.; Neumann, R.; Ensinger, W. Logic Gates Using Nanofluidic Diodes Based on Conical Nanopores Functionalized with Polyprotic Acid Chains. *Langmuir* **2009**, *25*, 11993–11997.
13. Wen, L.; Hou, X.; Tian, Y.; Zhai, J.; Jiang, L. Bio-Inspired Photoelectric Conversion Based on Smart-Gating Nanochannels. *Adv. Funct. Mater.* **2010**, *20*, 2636–2642.
14. Siwy, Z.; Fuliński, A. Fabrication of a Synthetic Nanopore Ion Pump. *Phys. Rev. Lett.* **2002**, *89*, 198103/1–198103/4.
15. Zhang, H.; Hou, X.; Zeng, L.; Yang, F.; Li, L.; Yan, D.; Tian, Y.; Jiang, L. Bioinspired Artificial Single Ion Pump. *J. Am. Chem. Soc.* **2013**, 10.1021/ja4037669.
16. Wang, G.; Zhang, B.; Wayment, J. R.; Harris, J. M.; White, H. S. Electrostatic-Gated Transport in Chemically Modified Glass Nanopore Electrodes. *J. Am. Chem. Soc.* **2006**, *128*, 7679–7686.
17. Momotenko, D.; Girault, H. H. Scan-Rate-Dependent Ion Current Rectification and Rectification Inversion in Charged Conical Nanopores. *J. Am. Chem. Soc.* **2011**, *133*, 14496–14499.
18. Schoch, R. B.; Han, J.; Renaud, P. Transport Phenomena in Nanofluidics. *Rev. Mod. Phys.* **2008**, *80*, 839–883.
19. Cervera, J.; Schiedt, B.; Neumann, R.; Mafá, S.; Ramírez, P. Ionic Conduction, Rectification, and Selectivity in Single Conical Nanopores. *J. Chem. Phys.* **2006**, *124*, 104706/1–104706/9.
20. Yameen, B.; Ali, M.; Neumann, R.; Ensinger, W.; Knoll, W.; Azzaroni, O. Single Conical Nanopores Displaying Ph-Tunable Rectifying Characteristics. Manipulating Ionic Transport with Zwitterionic Polymer Brushes. *J. Am. Chem. Soc.* **2009**, *131*, 2070–2071.
21. Kosińska, I. D.; Goychuk, I.; Kostur, M.; Schmid, G.; Hänggi, P. Rectification in Synthetic Conical Nanopores: A One-Dimensional Poisson-Nernst-Planck Model. *Phys. Rev. E: Stat., Nonlinear, Soft Matter Phys.* **2008**, *77*, 031131/1–031131/10.

22. Yameen, B.; Ali, M.; Neumann, R.; Ensinger, W.; Knoll, W.; Azzaroni, O. Proton-Regulated Rectified Ionic Transport through Solid-State Conical Nanopores Modified with Phosphate-Bearing Polymer Brushes. *Chem. Commun. (Cambridge, U.K.)* **2010**, *46*, 1908–1910.
23. Cervera, J.; Schiedt, B.; Ramírez, P. A Poisson/Nernst-Planck Model for Ionic Transport through Synthetic Conical Nanopores. *Europhys. Lett.* **2005**, *71*, 35–41.
24. Siwy, Z.; Kosińska, I. D.; Fuliński, A.; Martin, C. R. Asymmetric Diffusion through Synthetic Nanopores. *Phys. Rev. Lett.* **2005**, *94*, 048102/1–048102/4.
25. Ali, M.; Ramirez, P.; Nguyen, H. Q.; Nasir, S.; Cervera, J.; Mafe, S.; Ensinger, W. Single Cigar-Shaped Nanopores Functionalized with Amphoteric Amino Acid Chains: Experimental and Theoretical Characterization. *ACS Nano* **2012**, *6*, 3631–3640.
26. Vlassiouk, I.; Siwy, Z. S. Nanofluidic Diode. *Nano Lett.* **2007**, *7*, 552–556.
27. Cheng, L.-J.; Guo, L. J. Ionic Current Rectification, Breakdown, and Switching in Heterogeneous Oxide Nanofluidic Devices. *ACS Nano* **2009**, *3*, 575–584.
28. Ramírez, P.; Gómez, V.; Cervera, J.; Schiedt, B.; Mafé, S. Ion Transport and Selectivity in Nanopores with Spatially Inhomogeneous Fixed Charge Distributions. *J. Chem. Phys.* **2007**, *126*, 194703/1–194703/9.
29. Yan, R.; Liang, W.; Fan, R.; Yang, P. Nanofluidic Diodes Based on Nanotube Heterojunctions. *Nano Lett.* **2009**, *9*, 3820–3825.
30. Kalman, E. B.; Vlassiouk, I.; Siwy, Z. S. Nanofluidic Bipolar Transistors. *Adv. Mater. (Weinheim, Ger.)* **2008**, *20*, 293–297.
31. Vlassiouk, I.; Smimov, S.; Siwy, Z. Nanofluidic Ionic Diodes. Comparison of Analytical and Numerical Solutions. *ACS Nano* **2008**, *2*, 1589–1602.
32. Tagliazucchi, M.; Rabin, Y.; Szleifer, I. Ion Transport and Molecular Organization Are Coupled in Polyelectrolyte Modified Nanopores. *J. Am. Chem. Soc.* **2011**, *133*, 17753–17763.
33. Tagliazucchi, M.; Azzaroni, O.; Szleifer, I. Responsive Polymers End-Tethered in Solid-State Nanochannels: When Nanoconfinement Really Matters. *J. Am. Chem. Soc.* **2010**, *132*, 12404–12411.
34. Krapf, D.; Wu, M. Y.; Smeets, R. M. M.; Zandbergen, H. W.; Dekker, C.; Lemay, S. G. Fabrication and Characterization of Nanopore-Based Electrodes with Radii Down to 2 nm. *Nano Lett.* **2006**, *6*, 105–109.
35. Storm, A. J.; Chen, J. H.; Ling, X. S.; Zandbergen, H. W.; Dekker, C. Fabrication of Solid-State Nanopores with Single-Nanometre Precision. *Nat. Mater.* **2003**, *2*, 537–540.
36. Ricci, A. M.; Tagliazucchi, M.; Calvo, E. J. Charge Regulation in Redox Active Monolayers Embedded in Proton Exchanger Surfaces. *Phys. Chem. Chem. Phys.* **2012**, *14*, 9988–9995.
37. Vlassiouk, I.; Smirnov, S.; Siwy, Z. Ionic Selectivity of Single Nanochannels. *Nano Lett.* **2008**, *8*, 1978–1985.
38. Powell, M. R.; Vlassiouk, I.; Martens, C.; Siwy, Z. S. Nonequilibrium 1/F Noise in Rectifying Nanopores. *Phys. Rev. Lett.* **2009**, *103*, 248104/1–248104/4.
39. Hoogerheide, D. P.; Garaj, S.; Golovchenko, J. A. Probing Surface Charge Fluctuations with Solid-State Nanopores. *Phys. Rev. Lett.* **2009**, *102*, 256804/1–256804/4.
40. Sonnefeld, J. Determination of Surface Charge Density Parameters of Silicon Nitride. *Colloids Surf., A* **1996**, *108*, 27–31.
41. Stein, D.; Kruithof, M.; Dekker, C. Surface-Charge-Governed Ion Transport in Nanofluidic Channels. *Phys. Rev. Lett.* **2004**, *93*, 035901/1–035901/4.
42. Yameen, B.; Ali, M.; Neumann, R.; Ensinger, W.; Knoll, W.; Azzaroni, O. Synthetic Proton-Gated Ion Channels *Via* Single Solid-State Nanochannels Modified with Responsive Polymer Brushes. *Nano Lett.* **2009**, *9*, 2788–2793.
43. Hou, X.; Liu, Y. J.; Dong, H.; Yang, F.; Li, L.; Jiang, L. A pH-Gating Ionic Transport Nanodevice: Asymmetric Chemical Modification of Single Nanochannels. *Adv. Mater. (Weinheim, Ger.)* **2010**, *22*, 2440–2443.
44. Wen, L. P.; Hou, X.; Tian, Y.; Nie, F. Q.; Song, Y. L.; Zhai, J.; Jiang, L. Bioinspired Smart Gating of Nanochannels toward Photoelectric-Conversion Systems. *Adv. Mater. (Weinheim, Ger.)* **2010**, *22*, 1021–1024.
45. Jones, D. M.; Brown, A. A.; Huck, W. T. S. Surface-Initiated Polymerizations in Aqueous Media: Effect of Initiator Density. *Langmuir* **2002**, *18*, 1265–1269.
46. Peleg, O.; Tagliazucchi, M.; Kroeger, M.; Rabin, Y.; Szleifer, I. Morphology Control of Hairy Nanopores. *ACS Nano* **2011**, *5*, 4737–4747.
47. Tagliazucchi, M.; Peleg, O.; Kröger, M.; Rabin, Y.; Szleifer, I. Effect of Charge, Hydrophobicity, and Sequence of Nucleoporins on the Translocation of Model Particles through the Nuclear Pore Complex. *Proc. Natl. Acad. Sci. U.S.A.* **2013**, *110*, 3363–3368.
48. Widom, B. Some Topics in the Theory of Fluids. *J. Chem. Phys.* **1963**, *39*, 2808–2812.
49. Fang, F.; Szleifer, I. Controlled Release of Proteins from Polymer-Modified Surfaces. *Proc. Natl. Acad. Sci. U.S.A.* **2006**, *103*, 5769–5774.
50. Longo, G. S.; Olvera de la Cruz, M.; Szleifer, I. Molecular Theory of Weak Polyelectrolyte Thin Films. *Soft Matter* **2012**, *8*, 1344–1354.
51. Tagliazucchi, M.; Calvo, E. J.; Szleifer, I. Molecular Theory of Chemically Modified Electrodes by Redox Polyelectrolytes under Equilibrium Conditions: Comparison with Experiment. *J. Phys. Chem. C* **2008**, *112*, 458–471.
52. Uline, M. J.; Longo, G. S.; Schick, M.; Szleifer, I. Calculating Partition Coefficients of Chain Anchors in Liquid-Ordered and Liquid-Disordered Phases. *Biophys. J.* **2010**, *98*, 1883–1892.
53. Liu, Q.; Wang, Y.; Guo, W.; Ji, H.; Xue, J.; Ouyang, Q. Asymmetric Properties of Ion Transport in a Charged Conical Nanopore. *Phys. Rev. E: Stat., Nonlinear, Soft Matter Phys.* **2007**, *75*, 051201/1–051201/6.
54. Li, J.; Stein, D.; McMullan, C.; Branton, D.; Aziz, M. J.; Golovchenko, J. A. Ion-Beam Sculpting at Nanometre Length Scales. *Nature* **2001**, *412*, 166–169.
55. Martin, C. R. Nanomaterials: A Membrane-Based Synthetic Approach. *Science* **1994**, *266*, 1961–1966.
56. Hwang, W. L.; Holden, M. A.; White, S.; Bayley, H. Electrical Behavior of Droplet Interface Bilayer Networks: Experimental Analysis and Modeling. *J. Am. Chem. Soc.* **2007**, *129*, 11854–11864.
57. Holden, M. A.; Needham, D.; Bayley, H. Functional Bionetworks from Nanoliter Water Droplets. *J. Am. Chem. Soc.* **2007**, *129*, 8650–8655.
58. Lebon, G.; Jou, D.; Cases-Vázquez , J. *Understanding Non-Equilbirium Thermodynamics*; Springer-Verlag: Berlin, 2008.
59. Prigogine, I., *Introduction to Thermodynamics of Irreversible Processes*; Interscience Publishers: New York, 1955.